
Article:
Badran, Ghadeer, Lazarov, Vlado K. and Dhimish, Mahmoud (2026) Extending Photovoltaic Module Lifetime Through Targeted Repair of Short-Circuited Bypass Diodes. Solar. 4. ISSN: 2673-9941

https://doi.org/10.3390/solar6010004

---

solar

MDPI

Article

Extending Photovoltaic Module Lifetime Through Targeted Repair of Short-Circuited Bypass Diodes

Ghadeer Badran [1,*], Vlado K. Lazarov [1] and Mahmoud Dhimish [2]

[1] York-JEOL Nanocentre, University of York, York YO10 5BR, UK; vlado.lazarov@york.ac.uk
[2] Department of Electrical and Photonics Engineering, Technical University of Denmark, 4000 Roskilde, Sjælland, Denmark; mahdh@dtu.dk
* Correspondence: ghadeer.badran@york.ac.uk

Abstract

Bypass diode failure, particularly in the short-circuit mode, remains an under-addressed reliability issue in photovoltaic (PV) modules, causing severe power suppression and often leading to premature disposal of otherwise functional units. This study presents a non-destructive, field-applicable plug-in repair protocol for restoring modules affected by short-circuited bypass diodes. From twenty-two field-deployed modules, nine were analyzed in detail under healthy, single-fault, and dual-fault conditions. Controlled diode faults were introduced and subsequently repaired using commercially available plug-in bypass diodes. Electroluminescence (EL) imaging, current–voltage (I–V) testing, and extraction of series and shunt resistances were performed before and after repair. Results show that a single shorted diode deactivates one substring, reducing power by ~34–37%, while dual faults suppress over two-thirds of the active area, causing power losses above 67%. After repair, power deviation decreased to <3% for single faults and <7% for dual faults, with shunt resistance increasing by 52–262%, confirming removal of diode-induced leakage paths. Series resistance remained largely unchanged except in modules with irreversible cell-level damage accumulated during prolonged faulty operation. The findings demonstrate that short-circuited bypass diode faults are readily repairable and that component-level intervention can restore module performance, extend operational lifetime, and reduce unnecessary PV recycling.

Keywords: photovoltaics; bypass diodes; repair method; electroluminescent imaging; electrical performance; solar PV defect

Academic Editor: Jürgen Heinz Werner

Received: 3 November 2025
Revised: 28 November 2025
Accepted: 25 December 2025
Published: 6 January 2026

1. Introduction

Photovoltaic (PV) technology is widely recognized as a cornerstone in the global transition to sustainable energy. With its scalability, silent operation, and minimal maintenance requirements [1], PV has found application across residential rooftops, commercial buildings, and utility-scale solar farms [2]. The International Energy Agency (IEA) predicted that solar PV will become one of the dominant sources of electricity generation worldwide by the middle of this century [3]. However, this rapid expansion brings not only environmental benefits but also urgent challenges, particularly around PV reliability, fault management [4], and end-of-life (EoL) module disposal [5]. As the PV industry matures, attention must shift from simply deploying systems to sustaining them across their full lifecycle.

One emerging challenge is the growing volume of PV waste, with IRENA and IEA-PVPS reports indicating that PV waste is projected to reach between 60 million and

78 million tonnes globally by 2050 [6]. Although recycling processes exist, they are often constrained by low recovery values, largely due to trends in modern PV manufacturing, such as thinner silicon wafers and reduced silver content [7]. Consequently, there is increasing emphasis on repair-based strategies that aim to preserve the functional integrity of modules [8], extend their operational life, and minimise environmental impact. Many common PV defects, such as microcracks [9], delamination [10], solder joint failure [11], and potential-induced degradation (PID) [12], remain the focus of ongoing research aimed at improving detection and mitigation strategies. However, in cases where repair is technically feasible, it presents a more sustainable and cost-effective alternative to early module replacement or full recycling.

Among the various failure modes encountered in the field, bypass diode failure remains particularly underexplored despite its significant performance implications [13]. Bypass diodes are integrated into the module junction box to protect series-connected substrings from reverse bias under shading or mismatch conditions. As illustrated in Figure 1a, a typical PV module contains three such diodes, each covering 20-cell sub-strings.

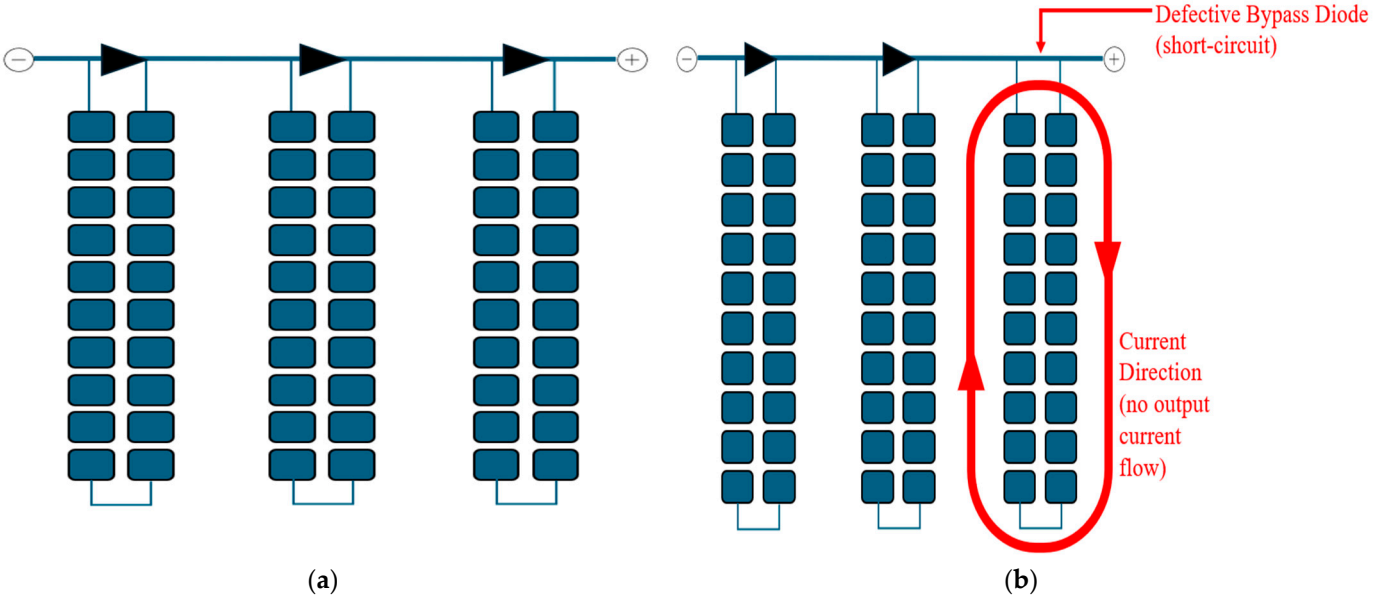

Figure 1. (**a**) Schematic of a standard PV module with three substrings and associated bypass diodes. (**b**) Effect of a short-circuited bypass diode in a PV module. When a bypass diode fails in short-circuit mode, it forms a permanent low-resistance path that bypasses its associated 20-cell substring.

While functioning diodes prevent overheating and enable safe current rerouting, one of the most frequent and problematic failure modes is the short-circuited bypass diode [14]. This condition creates a permanent low-resistance loop that bypasses the entire protected substring (as shown in Figure 1b), regardless of whether shading is present. As a result, all associated cells are excluded from energy conversion, often leading to a one-third loss in total module output. Critically, this type of failure leaves no external trace, making it difficult to detect without specialised diagnostic tools. Despite their field prevalence, bypass diode faults are rarely addressed from a repair perspective in academic or technical literature, with most studies focusing solely on detection [15–17].

A notable exception is the study by [18], which proposed an on-site resin-based recovery process targeting PV modules affected by resistive solder bond (RSB) hotspots. Uniquely, their methodology extended beyond fault detection to include the identification and replacement of short-circuited bypass diodes, a critical yet often overlooked failure mode. However, while the reported performance restoration (from ~62–65% to ~96–99% of

rated output) suggests promising results, closer validation reveals inconsistencies in the presented current–voltage (I–V) curves. Specifically, the presence of a defined knee point contradicts expectations for a module with a short-circuited bypass diode, where the entire affected substring should be electrically bypassed, leading to a flat segment or a one-third voltage drop. This discrepancy raises concerns about the accuracy of fault diagnosis or the effectiveness of the repair itself.

Short-circuited bypass diodes represent a distinct failure mode with a well-defined electrical signature. In this state, the diode presents near-zero impedance, resulting in a permanent low-resistance path across the protected substring [19]. Consequently, the current bypasses the entire 20-cell segment, irrespective of irradiance or shading conditions. This not only leads to a quantifiable voltage drop, typically around one-third of the module's nominal open-circuit voltage, but also suppresses power output from otherwise functional cells. Importantly, the short-circuit condition is passive and irreversible; unlike normal bypass operation triggered under reverse bias, a failed diode in short-circuit mode permanently disrupts the module's electrical topology.

Successful implementation depends on accurate fault localisation, for which electroluminescence (EL) imaging has proven essential [20,21]. Studies have demonstrated the high accuracy of EL imaging in detecting a wide range of PV defects, including microcracks, inactive regions, and bypass diode faults. When a reverse bias is applied through the EL testing, functional areas of a PV cell emit infrared radiation through radiative recombination, while inactive or defective regions appear dark [22–24]. In the case of a faulty bypass diode, this results in an entire substring failing to emit, allowing for rapid and non-destructive identification of the issue. As a result, EL imaging serves as a crucial diagnostic tool for both pre-repair fault detection and post-repair performance evaluation, particularly when complemented by I–V measurements.

Despite their critical protective role, failed bypass diodes, particularly those in short-circuit mode, are commonly treated as irreparable defects [25], often relegating otherwise functional PV modules to the recycling chain [26,27]. This industry practice overlooks the fundamental fact that bypass diodes are discrete, replaceable components, typically located within the junction box and accessible without disturbing the PV encapsulant layers.

2. Contribution of This Paper

This paper provides the first comprehensive experimental demonstration that PV modules affected by short-circuited bypass diodes can be effectively restored using a practical, non-destructive plug-in replacement method. Unlike existing approaches that require resin-based repair [18], thermal rework, or encapsulant removal [8], the proposed protocol enables rapid field implementation with minimal tools and no heating. By combining EL imaging and quantitative I–V characterization across modules with one or two diode faults, the study shows that power losses of ~34–37% (single bypass diode fault) and >67% (dual bypass diode fault) can be reduced to as little as 2.1% and below 6.5%, respectively, demonstrating that diode-level intervention can fully reinstate substring functionality under realistic field-aged conditions.

A further contribution is the use of resistive-parameter extraction to assess internal electrical restoration following repair. Shunt resistance increased by 52% to 262% across the modules, confirming the removal of low-impedance leakage paths associated with the shorted diodes, while series resistance remained largely stable, indicating no repair-induced resistive losses. By experimentally linking diode replacement to the recovery of power output, intrinsic electrical parameters, and module operability, this work establishes a validated framework for targeted component-level PV repair, offering a scalable pathway to extend module lifetime and reduce premature recycling and e-waste.

https://doi.org/10.3390/solar6010004

3. Materials and Methods

3.1. Repair Protocol for Bypass Diodes and Applied Diagnostic Methods

This study investigates the restoration potential of six crystalline silicon PV modules exhibiting one or two short-circuited bypass diodes, along with three additional modules containing fully functional bypass diodes. These latter modules serve as reference samples to benchmark the performance characteristics of non-defective systems under identical test conditions. Each module consists of 60 monocrystalline cells arranged in three substrings of 20 cells connected in series, as shown earlier in Figure 1a. Each substring is protected by a bypass diode, resulting in three diodes per module. The failure modes across the examined modules varied, with configurations showing one, two, or all three bypass diodes in a permanent short-circuit state. The electrical characteristics of the tested PV modules are summarized in Table 1.

Table 1. Electrical characteristics of the examined PV modules.

Parameter	Symbol	Value [1]
Maximum power	P_{max}	305 W
Maximum power voltage	V_{mp}	32.9 V
Maximum power current	I_{mp}	9.28 A
Open circuit voltage	V_{oc}	40.0 V
Short circuit current	I_{sc}	9.85 A

[1] Under standard test conditions (STC): irradiance = 1000 W/m^2, cell temperature 25 °C.

In this work, a total of twenty-two field-deployed PV modules were evaluated from a single operating string (see Figure 2a), of which nine were selected for detailed examination at the Technical University of Denmark (DTU). These modules were categorized into three main groups: Group 1 comprised three healthy reference modules with fully functional bypass diodes; Group 2 consisted of three modules each affected by one defective bypass diode; and Group 3 included three modules with two defective bypass diodes. The defective bypass conditions were deliberately created to replicate realistic short-circuit failures. This was achieved by carefully removing one or more diodes from the junction box using precision pliers (see Figure 2b) and bridging the connection terminals with a short conductive wire to establish a low-resistance path, as illustrated in Figure 2c. This configuration accurately reproduced the electrical behavior of a short-circuited bypass diode while maintaining the structural integrity of the module's circuitry.

To restore the functionality of these modules, a practical field-repair protocol was subsequently implemented. The procedure involved reopening the junction box and replacing the defective bypass diodes with new plug-in units. The PV modules were left outdoors for approximately 20 days after introducing bypass faults to simulate realistic field exposure and allow any early-stage degradation or thermal stress effects to manifest before repair.

As shown in Figure 2, each diode was mounted within a modular socket assembly that allows simple removal and replacement using handheld pliers, alongside a representative image of a typical PV module tested in this study. This method eliminates the need for desoldering, encapsulant removal, or thermal rework, making it highly suitable for on-site repairs. After diode replacement, each module was reassembled and resealed in preparation for post-repair diagnostic testing. The bypass diodes used for the repair were commercially available components of the same type originally installed in the modules, ensuring full electrical compatibility and straightforward plug-in replacement within the existing junction box terminals.

(**a**) (**b**) (**c**)

Figure 2. Photographs illustrating the experimental setup and bypass diode modification process: (**a**) field-deployed PV modules under evaluation; (**b**) removal of a bypass diode from the junction box using precision pliers to simulate a short-circuit fault; and (**c**) Junction box with two bypass diodes intentionally short-circuited to replicate dual-fault conditions.

Compared with existing repair approaches, such as resin-based hotspot recovery and diode-related interventions that require controlled indoor environments or thermal rework [18], as well as back sheet or encapsulant repairs that often involve partial disassembly of the module structure [8], the proposed plug-in bypass diode replacement method requires no heating, soldering, or encapsulant removal. This makes the protocol significantly more cost-effective, practical (takes approximately 5–7 min per module), and suitable for on-site field deployment. In contrast to these state-of-the-art methods, which typically require specialized equipment and labor-intensive handling, the present plug-in technique allows rapid component-level repair with minimal disruption to the module.

To assess the pre- and post-repair electrical integrity of each module, two complementary diagnostic techniques were employed: EL imaging and I–V curve tracing (summarized in Figure 3). EL imaging was conducted using a Nikon D3500 CMOS digital camera in a controlled low-light environment. The camera operated at a resolution of 1063 × 1771 pixels, with an exposure time of 6 s, ISO 100, and an aperture of f/1.8. A regulated power supply delivered a static forward bias current approximately equal to the module's rated short-circuit current (I_{sc}), ensuring optimal excitation of the cell material. This setup enables high-contrast imaging of internal defects, cracks, and inactive regions, particularly useful for detecting non-performing substrings associated with bypass diode failures. Imaging was performed before and after diode replacement to capture visual evidence of functional restoration. To avoid any thermal stress during EL imaging, particularly in PV modules containing inactive substrings, the forward-bias excitation was applied for a maximum duration of 30 s per capture, and EL images were taken immediately during this interval.

Electrical characterization was performed indoors using an Endeas 540XLi large-area AAA flasher equipped with Xenon lamps and a four-wire single-quadrant I–V measurement system with adjustable voltage bias. The flasher performed 10 ms forward sweeps (I_{sc} to V_{oc}) under a spectrum closely matched to AM1.5. All modules were left for several hours to stabilise in a temperature-controlled laboratory at 25 °C prior to testing, ensuring that each I–V curve was captured under STCs without the need for post-correction. This setup allows accurate and reproducible comparison of pre- and post-repair electrical performance.

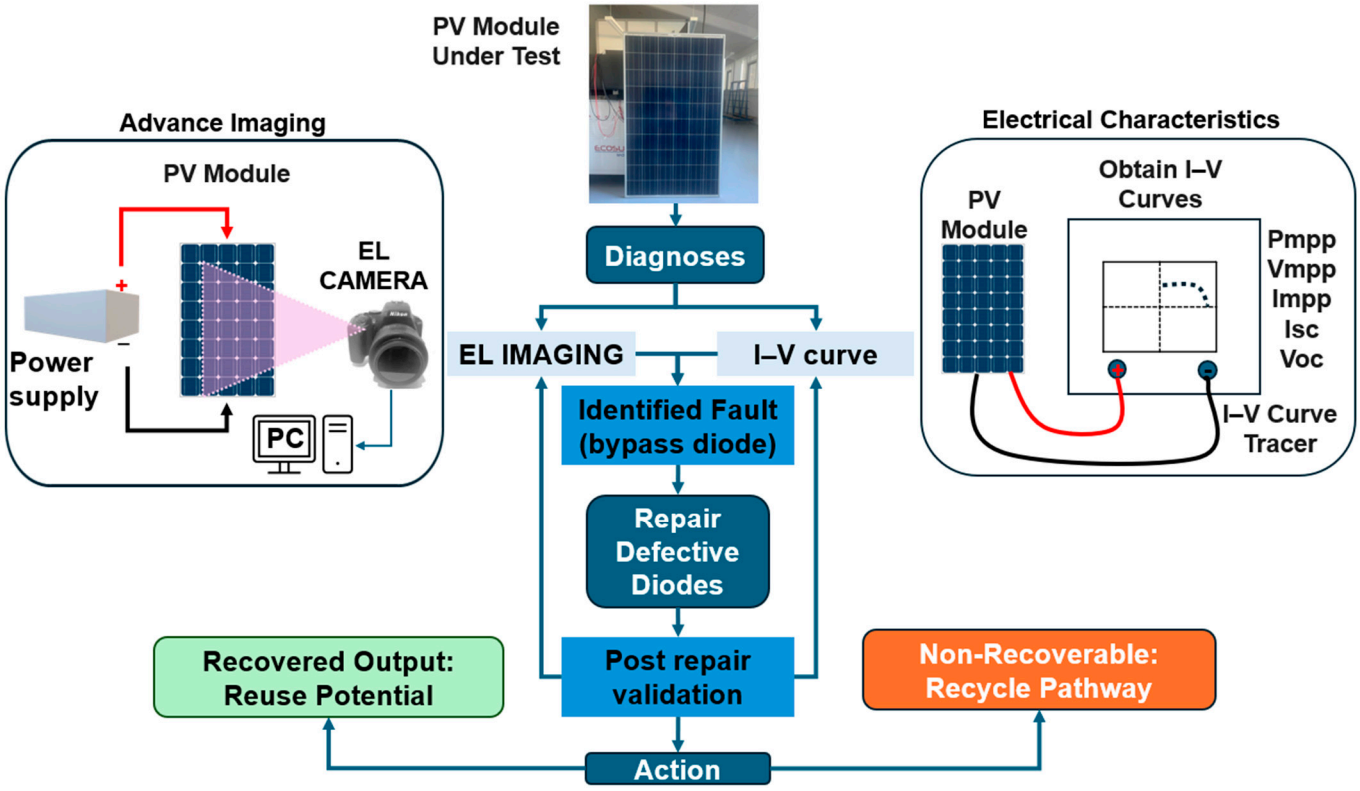

Figure 3. Schematic representation of the methodology used in this study to diagnose, repair, and validate PV modules affected by short-circuited bypass diodes.

3.2. Bypass Diode Electrical Behavior and Failure Implications

The electrical behavior of bypass diodes in a PV module can be approximated using the piecewise function of ideal diode conduction using (1). Where $V_{substring}$ is the voltage contribution of the i^{th} substring (each approximately one-third of the total module voltage), and Y_i is a binary condition function (1 if the substring is active, 0 if bypassed due to a shorted diode).

$$V_{module} = \sum_{i=1}^{3} V_{substring} \cdot Y_i \quad (1)$$

Under ideal conditions, all three substrings contribute, and the module voltage reaches its nominal rating (e.g., ~32.9 V for a 60-cell module in the tested PV modules). If one diode is permanently shorted, the current bypasses the associated substring entirely, resulting in a ~33% voltage reduction. However, actual I–V behavior can deviate from this simplified expectation due to parasitic resistances [28], partial activation of defective cells, or complex feedback between irradiance, temperature, and internal bypass conduction. Therefore, while a one-third voltage loss is theoretically expected, field measurements (such as those captured in this study) are crucial for understanding real-world deviations and validating repair outcomes.

It is worth mentioning that (1) provides only a first-order approximation of substring voltage contribution. It does not account for parasitic resistances, partial activation, reverse-bias leakage, or temperature-dependent effects. These limitations are addressed in Section 4.4 through extraction of series and shunt resistance parameters, offering a more complete characterization of internal electrical behavior.

In addition to electrical performance degradation (e.g., output maximum voltage), bypass diode failures have significant thermal and reliability implications. A short-circuited bypass diode allows continuous current flow through a low-impedance path, which not only removes the affected substring from contributing power but also increases the risk of

localized heating due to resistive losses in interconnects or solder bonds. Prolonged thermal cycling under such conditions can accelerate PV degradation mechanisms in surrounding materials, such as encapsulant browning [29], delamination [30], or corrosion [31].

4. Results

4.1. EL Imaging: Reference/Healthy Modules vs. Defective Modules (Short Circuit Bypass Diodes)

The EL images of the three reference modules (Modules#1–#3) are shown in Figure 4, which serve as baseline cases for performance comparison. These modules exhibit uniform luminescence across all substrings, indicating complete photoactive areas with no internal defects or inactive regions, as seen in Figure 4 EL images. The absence of dark substrings confirms full functionality of the bypass diodes and electrical continuity across all 60 cells in each module.

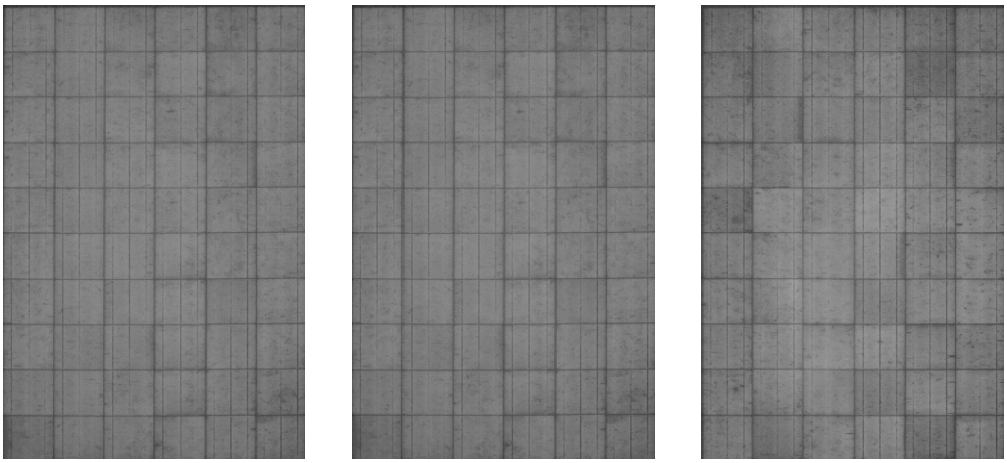

(**a**) (**b**) (**c**)

Figure 4. EL images of the reference (defective-free) PV modules: (**a**) Module#1; (**b**) Module#2; (**c**) Module#3.

In contrast, Figure 5 presents EL images of Modules#4–#6, each affected by a single short-circuited bypass diode. These faults result in a complete loss of luminescence across one substring per module, manifesting as vertically aligned dark bands. Specifically, Module#4 shows deactivation of the rightmost substring, corresponding to a third-diode failure; Module#5 exhibits loss in the central substring due to a middle-diode short; and Module#6 shows a completely dark leftmost substring, linked to a failure in the first diode. These patterns validate the correlation between diode short-circuit location and the corresponding inactive region, affirming EL imaging as a precise tool for localizing such faults.

More severe cases in which two bypass diodes are short-circuited are shown in Figure 6. As expected, Modules#7–#9 exhibit two completely dark substrings each, resulting in a visibly reduced active area. Module#7 shows a non-luminescent middle and right substring, Module#8 reveals deactivation of the first and middle substrings, while Module#9 is characterized by inactive left and right substrings. These patterns are consistent with the theoretical expectation that each short-circuited diode fully deactivates the corresponding substring, rendering it incapable of radiative recombination during forward bias operation.

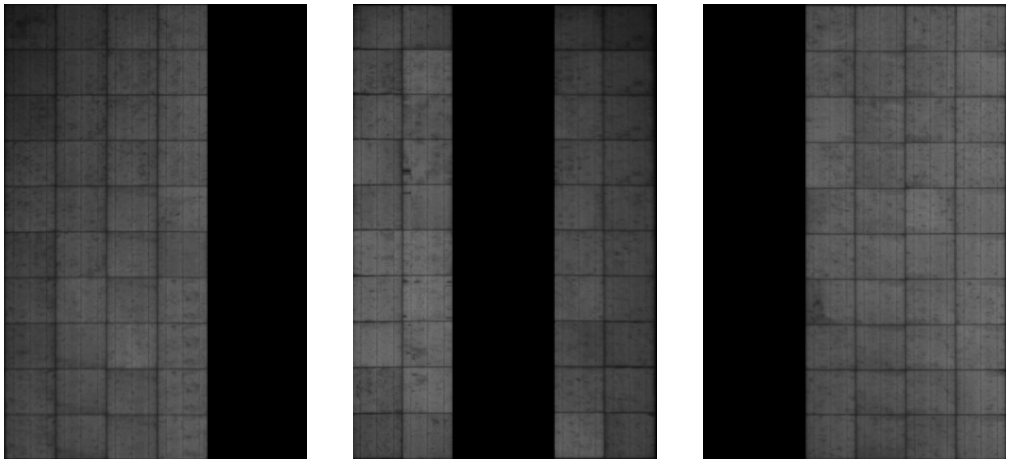

(**a**) (**b**) (**c**)

Figure 5. EL images of the PV modules affected by one short-circuit bypass diode: (**a**) Module#4, third bypass diode is shorted; (**b**) Module#5, middle bypass diode is shorted; (**c**) Module#6, first bypass diode is shorted.

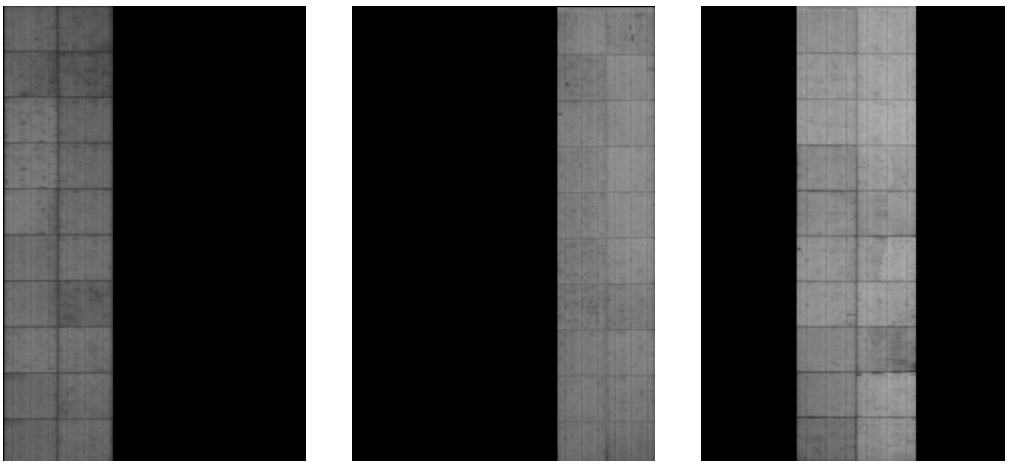

(**a**) (**b**) (**c**)

Figure 6. EL images of the PV modules affected by one short-circuit bypass diode: (**a**) Module#7, second and third bypass diode is shorted; (**b**) Module#8, first and second bypass diode is shorted; (**c**) Module#9, first and third bypass diode is shorted.

4.2. EL Imaging: Post-Repair EL Validation

The first set of post-repairs EL results correspond to the PV modules initially affected by a single faulty bypass diode. As shown in Figure 7a, the repair interventions, specifically the replacement of the defective bypass diodes, were successful, with all modules exhibiting a substantially improved EL profile. While a minor variation in luminescence remains detectable in the previously defective sub-strings, these differences are minimal and not indicative of persistent or severe degradation. The uniformity observed across the majority of cells suggests effective electrical reconnection and recovery. Notably, there is no evidence of corrosion, discoloration, defects, or new crack propagation, indicating that the repair did not introduce additional structural stress. The EL results serve as strong visual confirmation of electrical restoration; however, for a complete performance evaluation, the corresponding I–V characteristics pre- and post-repair will be analyzed in the following section.

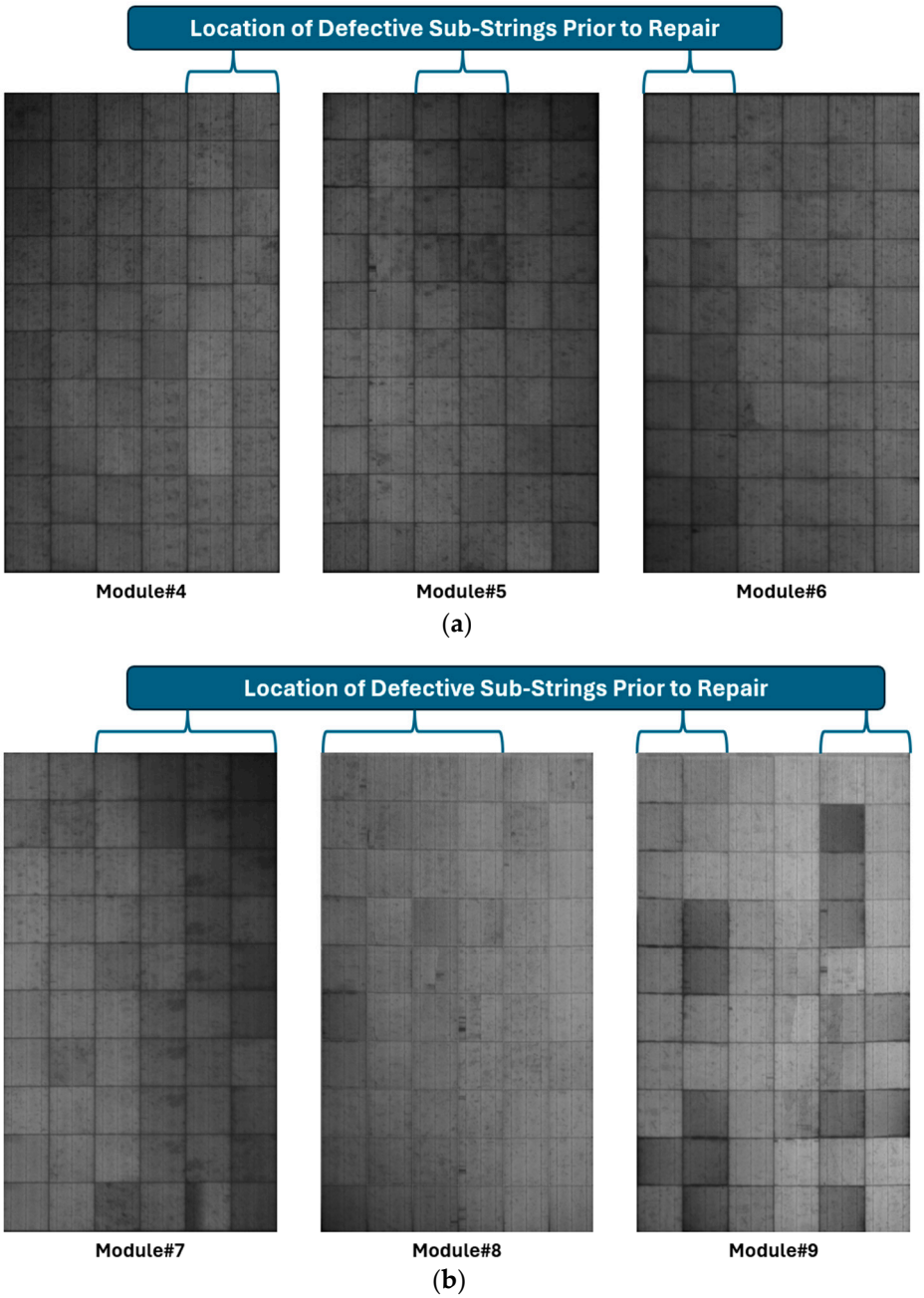

Figure 7. Post-repair EL images: (**a**) PV modules #4–#6, where all affected by one short-circuited bypass diode, (**b**) PV modules #7–#9, where all affected by two short-circuited bypass diodes.

We now turn our attention to the post-repair EL results of PV Modules#7–#9, each of which initially exhibited two short-circuited bypass diodes—a more severe fault condition compared to Modules#4–#6. As illustrated in Figure 7a,b, the EL signal has been largely restored in all three modules following the repair intervention, indicating that current flow through the sub-strings has resumed. However, the extent of damage and the effectiveness of the repair vary notably across the three cases.

In Module#7, although the EL image shows a general restoration of luminescence, approximately 11 individual cells exhibit signs of persistent darkening, indicative of localized degradation, most likely cell corrosion or interconnect damage. This suggests that the extended operation under faulty bypass diode conditions led to severe current crowding in the remaining functional sub-string. When a bypass diode is shorted, the corresponding sub-string is effectively bypassed, concentrating the operating current through the remain-

ing active paths. This uneven current distribution over time likely caused thermal stress and accelerated degradation in the still-active cells, resulting in partial electroluminescence suppression visible post-repair.

In contrast, Module#8 demonstrates a successful recovery, with a uniformly restored EL signature and no significant evidence of residual cell-level damage. This module appears to have experienced minimal collateral impact during the bypass failure event. The repair of the bypass diodes effectively reinstated full-string functionality, a conclusion that will be further validated through I–V characterization presented in the next section.

It is important to note that the dark cells observed in the repaired modules, particularly in Module #7 and Module #9, did not originate from the repair process but from pre-existing irreversible damage. Before repair, two substrings in each of these modules were permanently bypassed, meaning they carried no current and therefore masked underlying defects. Once the bypass diodes were replaced and full current flow was restored, previously latent degradation became apparent. In these modules, the remaining active substring was forced to carry the entire module current during operation, which can induce severe current crowding, localized heating, and reverse-bias stress. These conditions accelerate the formation of micro-shunts and weakened busbars, all of which manifest as darker regions in EL imaging (see Figure 8). Thus, the clearer visibility of shunted or inactive cells after repair reflects the reactivation of the electrical path rather than any repair-induced deterioration.

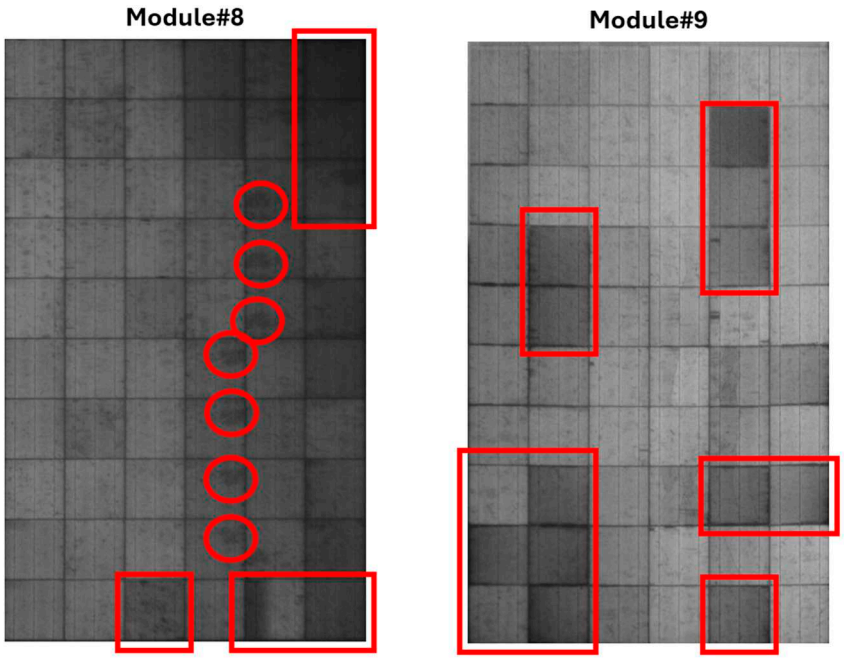

Figure 8. Post-repair EL images of Module#8 (**left**) and Module#9 (**right**). Red boxes and circles highlight regions exhibiting residual dark cells, micro-shunts, or inactive areas that became visible only after restoring current flow through the repaired bypass diodes.

4.3. I–V Characterization of PV Modules Before and After Repair of Short-Circuited Bypass Diodes

To evaluate the electrical degradation associated with short-circuited bypass diodes, the I–V curves of all PV modules were measured under standard test conditions (STC: 1000 W/m^2, 25 °C, AM1.5). The results are summarized in Figure 9, where Modules#1–#3 represent healthy baseline performance and Modules#4–#9 illustrate various levels of degradation prior to repair.

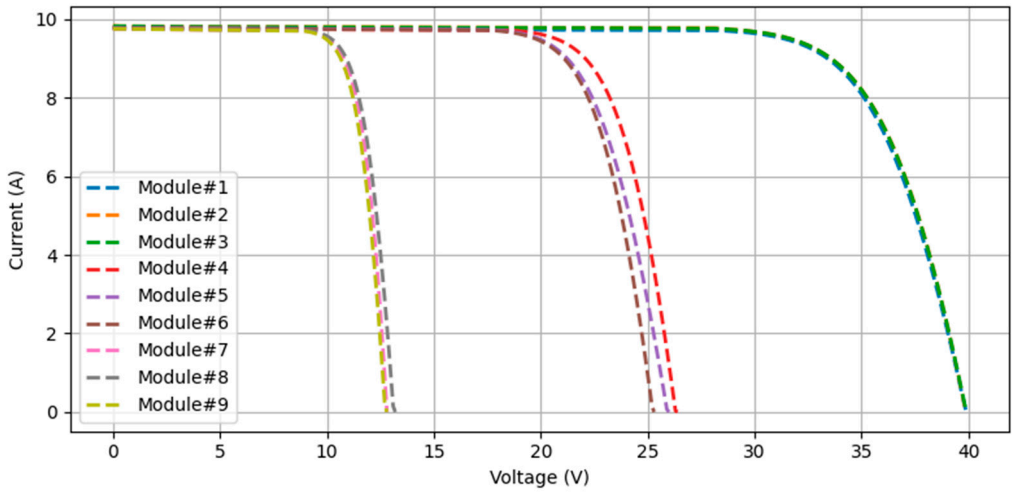

Figure 9. Measured I–V curves of PV modules before repair.

The modules with only one short-circuited bypass diode (#4–#6) show a noticeable but partial voltage drop, with open-circuit voltage (V_{oc}) and voltage at maximum power point (V_{mp}) reduced by approximately one-third. In contrast, Modules#7–#9, which had two short-circuited bypass diodes, exhibit significantly larger voltage suppression, up to two-thirds of the total voltage is lost. This is attributed to the loss of electrical contribution from multiple sub-strings, each containing a non-functional bypass diode.

To quantify the extent of degradation, the percentage deviation (Δ) in each electrical parameter was calculated relative to the average values from the healthy modules (Modules#1–#3). The deviation for each parameter X is defined as (2), and the results are shown in Table 2. This comparison enables a baseline-normalized assessment of performance loss due to bypass diode failure.

$$\Delta X = \frac{X_{module} - X_{healthy\ avg}}{X_{healthy\ avg}} \cdot 100 \tag{2}$$

where $X \in \{I_{sc},\ I_{mp}, V_{mp}, V_{oc}, P_{max}\}$.

Table 2. Relative percentage deviation in electrical parameters of PV modules (#4–#9) before repair, calculated with respect to the mean values of the healthy reference modules (#1–#3).

Module	ΔI_{sc} (%)	ΔI_{mp} (%)	ΔV_{mp} (%)	ΔV_{oc} (%)	ΔP_{max} (%)
#4	0.0	0.0	−34.0	−33.8	−34.3
#5	−0.1	−0.2	−36.6	−34.0	−36.7
#6	0.0	−0.3	−36.8	−36.5	−37.2
#7	−0.2	−0.5	−67.6	−67.9	−67.9
#8	−0.1	−0.1	−67.3	−66.8	−67.4
#9	−0.2	−0.6	−67.9	−67.9	−68.2

Modules#4–#6 experienced moderate voltage degradation (~34–37%) with negligible changes in current output, indicating that the bypass diode failure affected only one sub-string while the remaining two were still conducting. Conversely, Modules#7–#9 exhibited severe voltage degradation (up to ~68%) and measurable reductions in current at the maximum power point (I_{mp}), suggesting that most of the current was routed through a single sub-string during operation, causing thermal and electrical stress in those cells. These results align well with the EL observations reported earlier in the previous sections, where Modules#7–#9 showed darker patterns in two-thirds of the module area.

Most critically, the power loss (ΔP_{max}) exceeded 67% for Modules#7–#9, which confirms substantial energy yield reduction and system-level inefficiencies caused by sustained bypass diode failure. These values underscore the importance of early detection and intervention in diode-related faults.

The I–V curves measured after the bypass diode replacements (see Figure 10) reveal a near-complete restoration of electrical performance across all defective modules. When benchmarked against the reference group (Modules#1–#3), the repaired modules exhibit tight convergence in output characteristics, with maximum deviations in key parameters remaining within 6.5%.

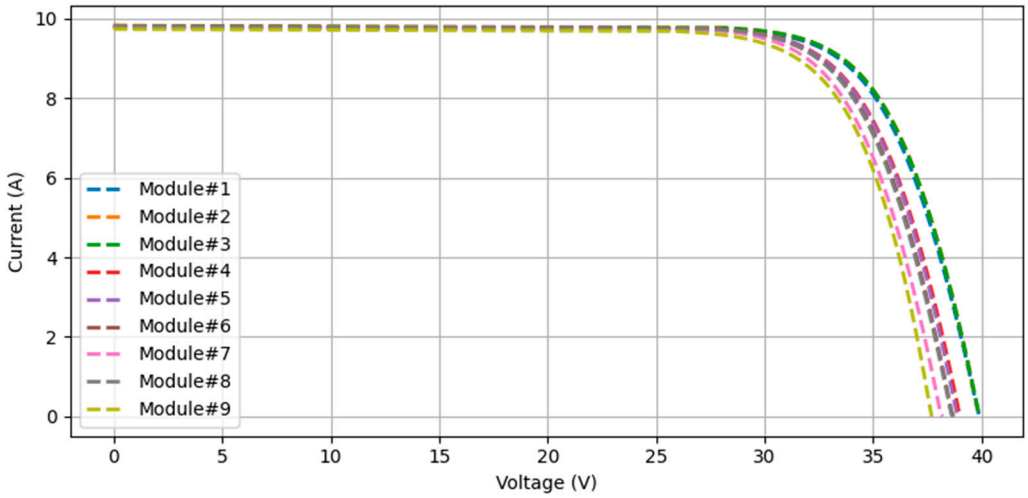

Figure 10. Measured I–V curves of PV modules post repairing the defective short-circuited bypass diodes in Modules#4–9. All modules demonstrate near-complete recovery in electrical performance.

Modules#4–#6, each originally affected by a single short-circuited bypass diode, show excellent recovery, with post-repair power output losses (ΔP_{max}) of only -2.1% to -2.9% (Table 3). Voltage-related deviations (ΔV_{oc}, ΔV_{mp}(%)) are similarly low ($\leq$3.1%), and current mismatches are negligible (<0.3%). This confirms that the electrical decoupling introduced by a single diode failure does not cause irreversible damage under short-term exposure, and that diode replacement alone is sufficient to reinstate module-level performance.

Table 3. Relative percentage deviation in electrical parameters of PV modules (#4–#9) after repair, calculated with respect to the mean values of the healthy reference modules (#1–#3).

Module	ΔI_{sc} (%)	ΔI_{mp} (%)	ΔV_{mp} (%)	ΔV_{oc} (%)	ΔP_{max} (%)
#4	−0.2	0.0	−1.9	−2.1	−2.1
#5	−0.1	−0.2	−2.1	−2.4	−2.2
#6	−0.1	0.0	−3.1	−3.1	−2.9
#7	−0.3	−0.3	−4.1	−4.2	−4.6
#8	−0.3	−0.4	−3.0	−2.6	−3.3
#9	−0.2	−1.1	−3.3	−5.1	−6.5

In contrast, Modules#7–#9, previously impacted by dual diode shorts, exhibit modest residual losses post-repair, with ΔP_{max} ranging from -3.3% to -6.5%. Although the I–V curves appear nominal at first glance, closer inspection reveals subtle impairments. Module#9 shows the highest deviation across nearly all parameters, notably a -5.1% drop in V_{oc} and -1.1% in I_{mp}, aligning with persistent inactive cells seen in its EL image. These observations suggest underlying cell-level degradation (e.g., interconnect corrosion, local

shunting, or irreversible thermal stress) likely sustained during extended field operation in a bypass-compromised state.

It is important to note that for Module #9, residual EL dark regions (as seen earlier in Figure 8) remained visible despite strong I–V recovery. In the next section (Section 4.4) will demonstrate that this module exhibited the largest increase in series resistance and reduced shunt resistance, indicating irreversible cell-level degradation accumulated during extended operation with two shorted bypass diodes. These latent defects become visible in EL once the current path is restored but have only a modest impact on overall module power, explaining the apparent discrepancy between EL and I–V behavior.

The ability to reduce power loss from ~68% (pre-repair) to less than 7% (post-repair) is a significant finding, reinforcing the effectiveness of targeted bypass diode repair even in modules with advanced degradation stages. Moreover, the current–voltage recovery profile highlights the electrical resilience of PV modules under well-executed maintenance protocols. From a PV system diagnostics perspective, the results underscore that while EL imaging is a valuable tool for fault localization, it must be supplemented by quantitative I–V evaluation to validate functional recovery. Residual mismatches in I–V performance may reveal latent defects not fully visible in EL patterns, particularly under scenarios of repeated or prolonged diode activation.

4.4. Extraction and Interpretation of Series and Shunt Resistances from I–V Characteristics

To complement the EL and I–V analyses presented in the previous sections, the electrical health of each module was further evaluated through the extraction of its series resistance (R_s) and shunt resistance (R_{sh}). These parameters provide deeper insight into the internal electrical pathways of the module and help assess whether the bypass diode repair restored not only the global I–V performance but also the intrinsic resistive behavior of the cell strings.

The resistances R_s and R_{sh} were derived directly from the measured I–V curves using a linear differential approach. This technique is grounded in the PV equivalent circuit model, in which R_s represents the resistive components in the current path, including metallization fingers, busbars, solder joints, and interconnect ribbons, while R_{sh} models leakage pathways, such as cell-to-cell shunts, microcracks, or diode-induced conduction. To compute both resistances, the following widely accepted approximations were used:

1. Series resistance (R_s) was obtained from the inverse slope of the I–V curve in the low-current region, specifically near open-circuit conditions (V_{oc}). In this regime, the derivative $-dV/dI$ captures the effective resistive drop as the current approaches zero, providing a robust estimate of the series-associated voltage losses. The typical value of healthy PV module series resistance is between 0.1 and 0.5 Ω.
2. Shunt resistance (R_{sh}) was calculated from the inverse slope of the I–V curve close to short-circuit conditions (I_{sc}). Here, the slope $-dV/dI$ reflects the degree of leakage or alternate current paths in the solar cells. A higher R_{sh} indicates fewer parasitic conduction paths and therefore better cell integrity, usually in the range between 200 and 700 Ω.

The extracted resistance values for each defective module, before and after bypass diode replacement, are presented in Table 4. The results reveal several notable trends. First, R_{sh} improved substantially across all modules following repair, with increases ranging from approximately 52% (Module#5) up to more than 260% (Module#4) depending on the severity of the original diode fault. This strong improvement confirms that the short-circuited bypass diodes had introduced significant low-resistance leakage paths across the associated substrings. When a diode fails in short-circuit mode, the affected substring becomes permanently bypassed, leading to reverse leakage and parasitic conduction channels that

manifest as reduced R_{sh}. Replacing the faulty diodes removes these shunt pathways, restoring the electrical isolation between cells and allowing R_{sh} to return to values characteristic of healthy modules.

Table 4. Extracted series resistance (R_s) and shunt resistance (R_{sh}) values of PV modules before and after bypass diode repair.

Module	R_s (Before)	R_s (After)	R_{sh} (Before)	R_{sh}
#4	0.28	0.29	173.3	627.4
#5	0.33	0.35	361.2	549.4
#6	0.27	0.31	287.7	474.8
#7	0.22	0.41	141.5	217.3
#8	0.26	0.29	275.1	552.4
#9	0.27	0.48	155.2	512.6

In contrast, the changes in R_s were relatively modest. For most modules, R_s increased slightly after repair, typically by only 0.01–0.04 Ω, which lies within normal measurement uncertainty for field I–V tracing. This is consistent with the physical expectation that bypass diode faults do not strongly affect the metallic conduction routes inside the module. However, Modules #7 and #9 displayed more pronounced increases in R_s, rising from 0.22 Ω to 0.41 Ω and from 0.27 Ω to 0.48 Ω, respectively. This behavior aligns with the EL observations shown earlier in Figure 8, where both modules exhibited multiple darkened cells and localized dark cells regions even after repair. These darker regions are likely associated with interconnect corrosion, or thermally stressed cells caused by prolonged operation with two short-circuited bypass diodes. Such cell-level degradation exacerbates resistive losses and results in higher effective R_s.

Overall, the resistance analysis reinforces the conclusions drawn from EL and I–V measurements. The bypass diode replacement successfully eliminated dominant shunt pathways, restoring R_{sh} to levels indicative of healthy cell behaviour, while the modest changes in R_s confirm that the repair process did not introduce additional resistive defects. The more noticeable increases in R_s observed in Modules #7 and #9 are attributed not to the repair itself but to pre-existing or irreversible degradation sustained during the extended faulty operating conditions. These findings underscore the importance of early bypass diode diagnosis and intervention to prevent long-term resistive damage.

5. Conclusions

This study provides the first comprehensive experimental demonstration that PV modules affected by short-circuited bypass diodes can be fully restored using a practical, non-destructive plug-in replacement method. Across nine representative modules with healthy, single-fault, and dual-fault conditions, the combined use of EL, AAA-class I–V characterization, and resistive-parameter extraction confirmed that short-circuited bypass diodes deactivate entire substrings, causing power losses of ~34–37% for single faults and over 67% for dual faults.

Following repair with commercially available bypass diodes, all modules exhibited full or near-complete recovery, with post-repair power deviations reduced to below 3% and 7% for single- and dual-fault modules, respectively. Shunt resistance increased by 52–262% after repair, demonstrating removal of diode-induced leakage paths, while series resistance remained largely stable, indicating that the intervention introduced no additional resistive defects. These results show that component-level repair is not only technically viable but also highly effective in restoring intrinsic PV performance, offering a scalable pathway to extend module lifetime, reduce unnecessary recycling, and improve the long-term reliability of solar assets.

Although the plug-in diode replacement demonstrated strong immediate electrical recovery, long-term reliability under thermal cycling, humidity exposure, and potential increases in contact resistance were not evaluated in this work. Future studies will include accelerated ageing tests (thermal cycling, damp-heat exposure, and field monitoring) to assess the durability of the plug-in diode–socket interface under real operating conditions over extended periods (e.g., 1–2 years of operation).

Author Contributions: Conceptualization, G.B.; methodology, G.B. and V.K.L.; validation, V.K.L. and M.D.; formal analysis, G.B.; resources, M.D.; data curation, G.B.; writing—original draft preparation, G.B.; writing—review and editing, V.K.L. and M.D.; supervision, V.K.L. All authors have read and agreed to the published version of the manuscript.

Funding: This research was funded by The Centre for Doctoral Training in Sustainable Materials for Net Zero at the School of Physics, Engineering and Technology, University of York.

Data Availability Statement: The raw data supporting the findings of this work are available from the corresponding author upon reasonable request.

Acknowledgments: The corresponding author, Ghadeer Badran, would like to thank the Technical University of Denmark (DTU) for hosting her from April to May 2025 and for providing access to their PV research facilities, which enabled the experiments reported in this work.

Conflicts of Interest: The authors declare no conflicts of interest.

References

1. Aboagye, B.; Gyamfi, S.; Ofosu, E.A.; Djordjevic, S. Investigation into the impacts of design, installation, operation and maintenance issues on performance and degradation of installed solar photovoltaic (PV) systems. *Energy Sustain. Dev.* **2022**, *66*, 165–176. [CrossRef]
2. Lopez, V.M.; Ziar, H.; Haverkort, J.W.; Zeman, M.; Isabella, O. Dynamic operation of water electrolyzers: A review for applications in photovoltaic systems integration. *Renew. Sustain. Energy Rev.* **2023**, *182*, 113407. [CrossRef]
3. Ahmed, R.; Reddy, G.V.; Singla, A.; Maan, P.; Dwivedi, S.P. A review paper on current state of the worldwide solar energy generation. In Proceedings of the E3S Web of International Conference on Futuristic Trends in Engineering, Science & Technology (ICFTEST-2024), Nagpur, India, 23–24 February 2024; EDP Sciences: Les Ulis, France, 2024; Volume 507, p. 01079.
4. Alimi, O.A.; Meyer, E.L.; Olayiwola, O.I. Solar photovoltaic modules' performance reliability and degradation analysis—A review. *Energies* **2022**, *15*, 5964. [CrossRef]
5. Badran, G.; Lazarov, V.K. From Waste to Resource: Exploring the Current Challenges and Future Directions of Photovoltaic Solar Cell Recycling. *Solar* **2025**, *5*, 4. [CrossRef]
6. Rozon, F.; McGregor, C.; Owen, M. Long-term forecasting framework for renewable energy technologies' installed capacity and costs for 2050. *Energies* **2023**, *16*, 6874. [CrossRef]
7. Popel', O.S.; Tarasenko, A.B. Modern development trends in photovoltaics. *Therm. Eng.* **2021**, *68*, 807–825. [CrossRef]
8. Voronko, Y.; Eder, G.C.; Breitwieser, C.; Mühleisen, W.; Neumaier, L.; Feldbacher, S.; Oreski, G.; Lenck, N. Repair options for PV modules with cracked backsheets. *Energy Sci. Eng.* **2021**, *9*, 1583–1595. [CrossRef]
9. Goudelis, G.; Lazaridis, P.I.; Dhimish, M. A review of models for photovoltaic crack and hotspot prediction. *Energies* **2022**, *15*, 4303. [CrossRef]
10. Hasan, A.A.; Alkahtani, A.A.; Shahahmadi, S.A.; Nur, E.; Alam, M.; Islam, M.A.; Amin, N. Delamination- and electromigration-related failures in solar panels—A review. *Sustainability* **2021**, *13*, 6882. [CrossRef]
11. Rabelo, M.; Zahid, M.A.; Agrawal, K.; Kim, K.; Cho, E.C.; Yi, J. Analysis of solder joint degradation and output power drop in silicon photovoltaic modules for reliability improvement. *Microelectron. Reliab.* **2021**, *127*, 114399. [CrossRef]
12. Badran, G.; Dhimish, M. Potential induced degradation in photovoltaic modules: A review of the latest research and developments. *Solar* **2023**, *3*, 322–346. [CrossRef]
13. Lee, C.G.; Shin, W.G.; Lim, J.R.; Kang, G.H.; Ju, Y.C.; Hwang, H.M.; Chang, H.S.; Ko, S.W. Analysis of electrical and thermal characteristics of PV array under mismatching conditions caused by partial shading and short circuit failure of bypass diodes. *Energy* **2021**, *218*, 119480. [CrossRef]
14. Fauzan, L.; Sim, Y.H.; Yun, M.J.; Choi, H.; Lee, D.Y.; Cha, S.I. Power from shaded photovoltaic modules through bypass-diode-assisted small-area high-voltage structures. *Renew. Sustain. Energy Rev.* **2025**, *208*, 115047. [CrossRef]

15. Dhimish, M.; Tyrrell, A.M. Photovoltaic bypass diode fault detection using artificial neural networks. *IEEE Trans. Instrum. Meas.* **2023**, *72*, 3507710. [CrossRef]
16. Ko, J.; Kim, C.; Lee, D.; Lee, S.; Shin, W.G.; Kang, G.H.; Oh, J.; Ko, S.W.; Song, H.J. Real-Time Detection and Classification of Bypass Diode-Related Faults in Photovoltaic Modules via Thermoelectric Devices. *Adv. Mater. Technol.* **2024**, *9*, 2301209. [CrossRef]
17. Baranwal, K.; Prakash, P.; Yadav, V.K. A modified bypass circuit for improved reliability of PV module validated with real-time data. *IEEE Trans. Device Mater. Reliab.* **2023**, *23*, 187–197. [CrossRef]
18. Lee, K.; Cho, S.B.; Yi, J.; Chang, H.S. Simplified recovery process for resistive solder bond (RSB) hotspots caused by poor soldering of crystalline silicon photovoltaic modules using resin. *Energies* **2022**, *15*, 4623. [CrossRef]
19. Rane, K.P.; Shiradkar, N. Long term durability assessment of Schottky bypass diodes in photovoltaic modules under high temperature reverse bias operation. *Sol. Energy* **2025**, *286*, 113152. [CrossRef]
20. del Prado Santamaría, R.; Dhimish, M.; dos Reis Benatto, G.A.; Kari, T.; Poulsen, P.B.; Spataru, S.V. From Indoor to Daylight Electroluminescence Imaging for PV Module Diagnostics: A Comprehensive Review of Techniques, Challenges, and AI-Driven Advancements. *Micromachines* **2025**, *16*, 437. [CrossRef]
21. Ozturk, E.; Ogliari, E.; Sakwa, M.; Dolara, A.; Blasuttigh, N.; Pavan, A.M. Photovoltaic modules fault detection, power output, and parameter estimation: A deep learning approach based on electroluminescence images. *Energy Convers. Manag.* **2024**, *319*, 118866. [CrossRef]
22. Redondo-Plaza, A.; Velasco-Bonilla, A.Z.; Morales-Aragones, J.I.; Zorita-Lamadrid, Á.L.; Alonso-Gómez, V.; Hernández-Callejo, L. Electroluminescence imaging based on FFT analysis for outdoor photovoltaic module inspection: A self-powered signal modulation approach. *Appl. Sci.* **2025**, *15*, 4606. [CrossRef]
23. Terrados, C.; González-Francés, D.; Alonso, V.; González, M.A.; Jiménez, J.; Martínez, O. Comparison of outdoor and indoor PL and EL images in Si solar cells and panels for defect detection and classification. *J. Electron. Mater.* **2023**, *52*, 5189–5198. [CrossRef]
24. Li, Y.; Wright, B.; del Prado Santamaría, R.; Liu, G.; Hameiri, Z. Robust denoising methodology for outdoor electroluminescence images of photovoltaic modules using deep learning. *Sol. Energy Mater. Sol. Cells* **2025**, *292*, 113750. [CrossRef]
25. Basnet, R.; Jones, L.; Azmie, M.A.; Jones, M.; McCann, M.; Ernst, M. Advancing Circular Economy of Silicon Photovoltaics: Current Status and Challenges of PV Module Reuse. *Sol. Energy Mater. Sol. Cells* **2025**, *292*, 113816. [CrossRef]
26. Al Zaabi, B.; Ghosh, A. Managing Photovoltaic Waste: Sustainable Solutions and Global Challenges. *Sol. Energy* **2024**, *283*, 112985. [CrossRef]
27. Mühleisen, W.; Brückner, M.; Neumaier, L. Investigation of Schottky Bypass Diodes from a Faulty PV Plant. *Sci. Technol. Energy Transit.* **2024**, *79*, 18. [CrossRef]
28. Tifidat, K.; Maouhoub, N.; Benahmida, A.; Salah, F.E.A. An accurate approach for modeling IV characteristics of photovoltaic generators based on the two-diode model. *Energy Convers. Manag. X* **2022**, *14*, 100205.
29. Bouguerra, S.; Agroui, K.; Kaaya, I.; Bouraiou, A.; Yaiche, M.R.; Mansour, D.E. Modeling the effect of PV module orientation on the encapsulant browning degradation rate in Algeria region. *IEEE J. Photovolt.* **2021**, *12*, 274–284. [CrossRef]
30. Meena, R.; Pareek, A.; Gupta, R. A comprehensive review on interfacial delamination in photovoltaic modules. *Renew. Sustain. Energy Rev.* **2024**, *189*, 113944. [CrossRef]
31. Sommeling, P.M.; Liu, J.; Kroon, J.M. Corrosion effects in bifacial crystalline silicon PV modules: Interactions between metallization and encapsulation. *Sol. Energy Mater. Sol. Cells* **2023**, *256*, 112321. [CrossRef]